3D-Printed Soft Magnetoelectric Microswimmers for Delivery and Differentiation of Neuron-Like Cells

Journal Article

Author(s):
Dong, Mei; Wang, Xiaopu; Chen, Xiang-Zhong; Mushtaq, Fajer; Deng, Siyu; Zhu, Caihong; Torlakcik, Harun; Terzopoulou, Anastasia; Qin, Xiao-Hua ⓘD; Xao, Xuanzhoing; Puigmarti-Luis, Josep; Choi, Hongsoo; Pêgo, Ana P.; Shen, Qun-Dong; Nelson, Bradley ⓘD; Pané, Salvador

3D-printed Soft Magnetoelectric Microswimmers for Delivery and Differentiation of Neuron-like Cells

Mei Dong, Xiaopu Wang, Xiang-Zhong Chen*, Fajer Mushtaq, Siyu Deng, Caihong Zhu, Harun Torlakcik, Anastasia Terzopoulou, Xiao-Hua Qin, Xuanzhong Xiao, Josep Puigmartí-Luis, Hongsoo Choi, Ana Paula Pêgo, Qun-Dong Shen*, Bradley J. Nelson, and Salvador Pané*

M. Dong, X. Xiao, Prof. Q.-D. Shen
Department of Polymer Science and Engineering and Key Laboratory of High Performance Polymer Materials and Technology of MOE, School of Chemistry and Chemical Engineering, Nanjing University, Nanjing 210023, China
E-mail: qdshen@nju.edu.cn

X. Wang, Dr. X.-Z. Chen, F. Mushtaq, H. Torlakcik, S. Deng, A.Terzopoulou, Prof. B. J. Nelson, and Dr. S. Pané
Multi-Scale Robotics Lab (MSRL), Institute of Robotics & Intelligent Systems (IRIS), ETH Zurich, Zurich 8092, Switzerland
E-mail: chenxian@ethz.ch; vidalp@ethz.ch

Dr. C.H. Zhu
Department of Neurobiology, School of Basic Medical Sciences, Fudan University, Shanghai, China

Dr. X.-H. Qin
Institute for Biomechanics, ETH Zurich, Leopold-Ruzicka-Weg 4, Zurich 8093, Switzerland

Dr. J. Puigmartí-Luis,
Institute of Chemical and Bioengineering, ETH Zurich, Vladimir Prelog Weg 1, 8093 Zurich, Switzerland

Prof. Hongsoo Choi
Department of Robotics Engineering and DGIST-ETH Microrobot Research Center, Daegu Gyeongbuk Institute of Science and Technology (DGIST), 42988, Daegu, South Korea

Prof. A. P. Pêgo
INEB – Instituto de Engenharia Biomédica, Universidade do Porto (UPorto), Rua Alfredo Allen 208, 4200-135 Porto, Portugal; i3S - Instituto de Investigação e Inovação em Saúde, UPorto, Portugal; ICBAS - Instituto de Ciências Biomédicas Abel Salazar, UPorto, Portugal; FEUP - Faculdade de Engenharia, UPorto, Portugal

Abstract:

Neurodegenerative diseases generally result in irreversible neuronal damage and neuronal death. Cell therapy shows promise as a potential treatment for these diseases. However, the therapeutic targeted delivery of these cells and the *in situ* provision of a suitable microenvironment for their differentiation into functional neuronal networks remains challenging. Here, we introduce a highly integrated multifunctional soft helical microswimmer featuring targeted neuronal cell delivery, on-demand localized wireless neuronal electrostimulation, and post-delivery enzymatic degradation. The helical soft body of the microswimmer is fabricated by two-photon lithography of the photocurable gelatin-methacryloyl (GelMA)-based hydrogel. The helical body is then impregnated with composite multiferroic nanoparticles displaying magnetoelectric features (MENPs). While the soft GelMA hydrogel chassis supports the cell growth, and is degraded by enzymes secreted by cells, the MENPs allow for the magnetic transportation of the bioactive chassis, and act as magnetically mediated electrostimulators of neuron-like cells. The unique combination of materials makes these microswimmers highly integrated devices that fulfill several requirements for their future translation to clinical applications, such as cargo delivery, cell stimulation and biodegradability. We envision that these devices will inspire new avenues for targeted cell therapies for traumatic injuries and diseases in the central nervous system.

1. Introduction

The pathogenesis of neurodegenerative disorders such as Parkinson's and Alzheimer's diseases, and traumatic injuries of the central nervous system usually result in the irreversible death of neurons.[1] Among treatments currently available such as conventional drug therapies, neurosurgery and gene therapy, cell treatment shows great potential for repairing the damaged tissue of the central nervous system.[2] Therapeutic cells, such as neural stem cells or neural progenitor cells, which can be induced to differentiate into neurons, are cultured *in vitro* and subsequently transplanted. However, the targeted delivery of these therapeutic cells and subsequent *in-situ* differentiation under appropriate stimulation remains challenging. Microrobotic devices show great potential for the minimally invasive treatment of diseases.[3] It has been demonstrated that these devices can deliver drugs to targeted regions, even *in vivo*, to perform therapeutic tasks. [3j, 4] For neuronal cell delivery, an ideal microrobot should also provide a suitable microenvironment to maintain important cellular functions. This microenvironment should approximate the physiological conditions of the soft extracellular matrix, as the differentiation of neuronal cells is influenced by the substrate stiffness.[5] Once their tasks have been completed, the safest way to remove these devices from the body is to let them degrade into nontoxic products that can be metabolized and/or excreted.[3a, 3c, 6] However, most of the reported cell-transporting microrobots are made of hard materials, which fail to provide a supportive and/or stimulating microenvironment for the cells, or to degrade once they have accomplished their delivery tasks.[7]

In this work, we propose an integrated soft magnetic microrobotic swimmer featuring neuronal cell delivery, in situ neuronal stimulation and biodegradation. The microswimmer is based on a 3D-printed biodegradable soft hydrogel microstructure, which provides a biocompatible substrate to support the cell growth, and will degrade after the delivery of the neuronal cells. A magnetic manipulation strategy was used, as magnetic fields are not harmful and can penetrate deep inside the human body.[3d, 8] Magnetoelectric nanoparticles (MENPs)

were integrated onto the microswimmers to serve as the motile components for magnetic actuation under low magnitude rotating magnetic fields. These MENPs, which convert magnetic input into electric output, [9] were also used to induce the differentiation of neuronal cells under electrostimulation. Utilizing a single energy source for navigating the microswimmer and triggering its stimulating function simplifies the design of the control platform.[3i, 10]

2. Results and Discussions

The fabrication of the microswimmer is schematically illustrated in **Figure 1**a. A photo-curable resin containing gelatin-methacryloyl (GelMA) as the precursor and sodium 3,39-((((1E,19E)-2-oxocyclopentane-1,3-diylidene) bis (methanylylidene))bis(4,1-phenylene)) bis(methylazanediyl)) dipropanoate (P2CK) as the photoinitiator, were selectively cross-linked by two-photon polymerization (TPP) to form specifically designed 3D microstructures.[6d, 6e] TPP, also known as direct laser writing (DLW), is an advanced 3D printing technique at microscale used for the controlled fabrication of microstructures with a variety of shapes.[11] In this work, we selected a helical shape which has been widely studied in the field of microrobotics as a vehicle for the controlled delivery of therapeutic agents. GelMA is a hydrogel showing excellent affinity to cells, so it supports cell adhesion, migration and proliferation,[6d, 12] and has been widely explored as scaffold material for 3D cell culture. More importantly, it can be degraded by the enzymes in the extracellular matrix (ECM) produced by the cells, and the degradation rate can be fine-tuned by changing the dimensions and shape of the structures. Therefore, GelMA was selected as the substrate material for the helical microswimmer. Figure 1b shows an optical microscope image showing several representative helical microstructures of various sizes made from cross-linked GelMA using TPP.

The helical microstructures were incubated in water dispersion of core-shell MENPs, which are composed of a $CoFe_2O_4$ (CFO) core and a $BiFeO_3$ (BFO) shell.[9b] The detailed preparation methods and characterization of these MENPs can be found in the supporting information (in

the experimental section, Figure S1 and associated discussion). The MENPs were adsorbed on the helical microstructures, forming a uniform layer, as shown in Figure 1c. The magnetism in the MENPs allows the helical microswimmers to be actuated using magnetic fields. When a rotating magnetic field is applied, the microswimmers rotate since the magnetic moment tends to align itself with the direction of the magnetic field, even if the magnitude of the field is as low as a few millitesla. The supporting information (Supporting Video SV1) shows the helical microswimmers can be actuated to rotate around their short axis, transforming the rotating motion into a translational motion under a rotating magnetic field. This actuation strategy has proven to be one of the most efficient propulsion methods in low Reynold number environments at the microscale, and can be compared to *E. Coli* bacteria propulsion using their flagella.[13] As a result of the friction between the microswimmer and the substrate surface, the microswimmer not only moves forward, but also drifts towards the lateral side. The relationship between the actuation frequency of external rotating magnetic fields, the size of the microswimmers, and the swimming speed can be found in the supporting information (Section 3, Figure S2-S4). For future clinical application, we propose to intrathecally inject our microswimmers by means of catheters, and then steer the microswimmers to the target site of implantation. In this case, the influence of lateral drift can be minimized when we actuate the microswimmer close to a physical boundary, for example, one of the walls of the subarachnoid space. In this situation, we can actuate the microswimmer to swim towards a targeted region, as shown in Supporting Video SV2 and Figure S5, which depicts a microswimmer moving along the wall of a microfluidic channel under actuation of a rotating magnetic field. We have tested the swimming behavior not only in DI water, but also in a body-simulated fluid such as artificial cerebrospinal fluid (CSF). CSF is a fluid that results from ultrafiltration of plasma. It possesses very low protein content and it is practically acellular. The viscosity of CSF is around 1 mPa·S, similar to that of water, and it is one of the few Newtonian fluids in the human body. As expected, we found that the environment of the artificial CSF did not compromise the swimming performance

of the microswimmer (Supporting Video SV3 and Figure S6). As we propose to deliver the neuronal cells with the microswimmer, it is also necessary to confirm the mobility of a microswimmer when it is loaded with cells. As shown in Figure 1d and Supporting Video SV4, a 100 μm long microswimmer was loaded with a neuronal cell (indicated by the white arrow in the inset) and actuated with a rotating magnetic field of 8 mT and 4 Hz to move along the wall of a microfluidic channel. The microfluidic channel was filled with phosphate-buffered saline (PBS) to simulate the microenvironment in a confined area such as that of the subarachnoid space. The viability of cells loaded on microswimmers after swimming was also confirmed through live-dead staining of the cells immediately after the swimming task in a cell culture plate, which indicates our microswimmer can safely keep the cells alive during the delivery process (Figure S7). Once the cells have been delivered to the target area, the helical microswimmers will be gradually degraded by the enzymes secreted by the surrounding cells (in this case proteinases), thereby releasing the therapeutic cells and the MENPs. Simultaneously, an alternating magnetic field will be applied to the system to stimulate the differentiation of the neuronal cells. When the MENPs are subjected to magnetic fields, the magnetostrictive CFO core will experience a strain, which will be exerted on the BFO shell, causing transient change in the surface charges of the nanoparticles. The change in the transient charge can be used to induce cell differentiation, as is schematically shown in **Figure 2**a. The human neuroblastoma cell line SH-SY5Y was selected to demonstrate the feasibility of the proposed concept, as this cell line is widely adopted for the study of neurodegenerative diseases. Figure 2b shows the optical microscope images of GelMA+MENPs microswimmers cultured with SH-SY5Y cells at varying intervals. The helical structures of the microswimmers gradually collapsed as time elapsed, and the primary construction completely disappeared after 7 days, suggesting that the helical microswimmers can be degraded by the proteinases produced by SH-SY5Y cells. In the meantime, the MENPs were also released, as evidenced by the black debris lying around. As the microswimmers are to be implanted into humans, it is essential to

confirm that they have good biocompatibility. MTT assays show that microswimmers and their degraded products, together with the MENPs, have negligible cytotoxicity to SH-SY5Y cells after culturing for 7 days (Figure 2c). In fact, the metabolic activity of the cells cultured with the GelMA was slightly higher (~15 %) than the control group, which further confirms that GelMA provides an excellent microenvironment for the cells. Caspase-3 (Cas-3) is regarded as one of the most typical proteases that is engaged in apoptosis of cells. It is normally inactive, but would be upregulated and activated when a cell undergoes apoptosis. Compared with negative control, neither GelMA nor MENPs significantly upregulated the expression of Cas-3, judging from the expression level of mRNA (Figure 2d) and the Western blot analysis (Figure 2e). The live-dead staining assays also confirm the biocompatibility of our microswimmers by showing negligible number of dead cells (Figure 2f), and even the cells in direct contact with the MENPs survived. Note that the biocompatibility of these nanoparticles has also been demonstrated in other cell lines such as MG63 osteosarcoma cells.[9b] We have also injected the MENPs to the striatum area of mice (n=6). After 15 days, all the mice survived, and no obvious inflammation or cellular damage was detected around the injection site compared to the contralateral hemisphere (as a control) (Figure S8). A recent report shows that Fe-based inorganic nanoparticles such as cobalt ferrite slowly degrade under physiological conditions. Intracellular ferritin cages localized nearby the nanoparticles could act as storage proteins for the metal ions released during the degradation.[14] These preliminary studies show promising application of the MENPs as a therapeutic agent. Note that further investigations are required to assess the long-term in vivo biosafety of MENPs, although these MENPs did not show acute toxicity under the investigated conditions.

The fact that the MENPs can induce neuronal differentiation of SH-SY5Y cells is another important reason that renders MENPs an interesting therapeutic agent. As is known, the pathogenesis of neurodegenerative diseases or neuron trauma is accompanied by the inevitable death of neurons. There are many challenges associated with the efficient induction of the

therapeutic cells (e.g. neural progenitor cells or stem cells) to form a functional neuronal network in the damaged area. One of the prerequisites for forming a functional neuronal network is the generation of axons and dendrites during differentiation. While the neuronal differentiation of the cells cultured with MENPs under magnetic stimulation with an alternating magnetic field was imperceptible after 3 days (Figure S9), obvious neuronal differentiation can be observed after 7 days (Figure S10). **Figure 3**a shows the fluorescent and bright field images of the cells cultured in different conditions after 10 days. While the control samples mostly remained undifferentiated, the cells experiencing differentiation conditions (i.e. GelMA + MENPs + Magnetic stimulation) exhibited extensive neurite outgrowth with multipolar shape. The number of SH-SY5Y cells under differentiation was less than the other control groups, which is consistent with previous reports that the proliferation of cells slows down during differentiation. The statistical results after normalization, i.e. the ratio of neurite number to the total cell number, was presented as a percentage ± the standard deviation, as shown in Figure 3b and Figure S10. We observed that cells cultured with MENPs under magnetic stimulation possess a higher percentage of differentiated multipolar cells (~40%) than those only receiving magnetic field stimulation (~10%), those only cultured with MENPs (~13%) (Figure 3b) and those cultured with CFO nanoparticles under magnetic stimulation (~13%) (Figure S11). Formation of neuronal cells in the negative control was rarely observed (~6%).

Morphological change, i.e. the extension of axons and dendrites, is only one of the prerequisites for a functional neuronal network. The signaling between the neuronal cells has to be realized by certain proteins. Therefore, it is necessary to further verify the differentiation of SH-SY5Y cells by examining certain functional proteins. For this purpose, we detected the expression level of Growth Associated Protein 43 (GAP43) in different groups. GAP43 is an axon membrane protein, which is a neuronal specific protein involved in extracellular growth and synaptic formation and regeneration of nerve cells.[15] It is expressed at a high level during the development and regeneration of neurons. The overexpression of GAP43 in a

neurodegenerative disease or a traumatic injury in a mouse model showed a significant improvement in the dysfunction of the mouse.[16] Figure 3c shows a pandect of immunofluorescence images of different groups after a culture of 10 days. The nuclei are fluorescently stained in blue and the GAP 43 in green. It is clear that the expression of GAP43 in SH-SY5Y cells cultured with GelMA + MENPs under magnetic stimulation is much higher than in the other three control groups. The fluorescence intensity of GAP43 was measured, and is presented in Figure 3d. We found that the level of GAP43 expression in SH-SY5Y cells cultured with GelMA + MENPs under magnetic field was ten times higher than the other groups. These results indicate that the microswimmers can not only deliver living cells under a magnetic field generated by direct current, but can also induce cell differentiation under an alternating magnetic field.

3. Conclusions

In this work, we propose an integrated microrobotic swimmer that is able to deliver neuronal cells and stimulate their differentiation. To this end, we fabricated 3D-printed helical microswimmers with biodegradable hydrogel GelMA as the substrate material and CFO@BFO magnetoelectric nanoparticles. The soft nature of the hydrogel provides a good basis for cell growth during transportation. Note that other degradable hydrogels could also suit this purpose, and the shape of the structures could be further optimized to better accommodate the cells and provide better maneuverability. We have seen other emerging hydrogel materials, which can maintain live organisms and cells while being 3D-printed. The MENPs not only serve as the motile components under rotating magnetic fields, but also as electric-field nanogenerators when subjected to alternating magnetic fields. Other investigations have reported that under ultrasonic stimulation, the charges generated by piezoelectric materials can be used to induce differentiation of neuronal cells.[5, 17] Our magnetoelectric stimulation could provide an alternative method of stimulating the neuronal cells in a less invasive and gentler manner. Physical stimulation, such as ultrasonic and magnetic stimulation, may potentially minimize

the use of expensive growth factors, when compared to other active cell delivery methods,[6e] thus providing a more cost-effective solution. In addition, utilizing the same energy source, in this case the magnetic fields, for both actuating the microswimmer and triggering its function, can simplify the instrument design. Although the long-term biosafety of MENPs needs further investigation, other alternative multiferroic materials are currently being investigated in terms of biocompatibility and cytotoxicity, and can be employed to replace the current MENPs if they are proven not to be suitable for clinical applications. Apart from materials safety, a proper in-vivo imaging technique, such as near - infrared imaging and X-ray fluoroscopy, should be developed and integrated for the in-vivo application of such microrobots. We believe that the proposed highly integrated microrobotic platform with magnetoelectric characteristics has the potential to enable new approaches for the treatment of trauma and diseases in the central nervous systems.

Supporting Information

Supporting Information is available from the Wiley Online Library or from the author.

References

[1]   a) K. A. Jellinger, *J. Neural Transm.* **2000**, *107*, 1; b) S. Majd, J. H. Power, H. J. Grantham, *BMC Neurosci.* **2015**, *16*, 69; c) K. A. Jellinger, C. Stadelmann, *J. Alzheimers Dis.* **2001**, *3*, 31.

[2]   a) J. S. Lunn, S. A. Sakowski, J. Hur, E. L. Feldman, *Ann. Neurol.* **2011**, *70*, 353; b) K. Sugaya, M. Vaidya, *Adv. Exp. Med. Biol.* **2018**, *1056*, 61.

[3]   a) Z. Wu, X. Lin, X. Zou, J. Sun, Q. He, *ACS Appl. Mater. Interface.* **2014**, *7*, 250; b) J. Li, B. E.-F. de Ávila, W. Gao, L. Zhang, J. Wang, *Sci. Robot.* **2017**, *2*, eaam6431; c) Y. Tu, F. Peng, A. A. André, Y. Men, M. Srinivas, D. A. Wilson, *ACS Nano* **2017**, *11*, 1957; d) B. J. Nelson, I. K. Kaliakatsos, J. J. Abbott, in *Annual Review of Biomedical Engineering*, Vol. 12 (Eds: M. L. Yarmush, J. S. Duncan, M. L. Gray), **2010**, 55; e) H. Wang, M. Pumera, *Chem. Rev.* **2015**, *115*, 8704; f) M. Medina-Sanchez, L. Schwarz, A. K. Meyer, F. Hebenstreit, O. G. Schmidt, *Nano Lett.* **2016**, *16*, 555; g) L. Zheng, L.-g. Chen, H.-b. Huang, X.-p. Li, L.-l. Zhang, *Microsyst. Technol.* **2016**, *22*, 2371; h) H. Ceylan, J. Giltinan, K. Kozielski, M. Sitti, *Lab Chip* **2017**, *17*, 1705; i) X.-Z. Chen, M. Hoop, N. Shamsudhin, T. Huang, B. Ozkale, Q. Li, E. Siringil, F. Mushtaq, L. Di Tizio, B. J. Nelson, S. Pané, *Adv. Mater.* **2017**, *29*, 1605458; j) X. Yan, Q. Zhou, M. Vincent, Y. Deng, J. Yu, J. Xu, T. Xu, T. Tang, L. Bian, Y.-X. J. Wang, K. Kostarelos, L. Zhang, *Sci. Robot.* **2017**, *2*, eaaq1155; k) X. Wang, C. Hu, L. Schurz, C. De Marco, X. Chen, S. Pane, B. J. Nelson, *ACS Nano* **2018**, 6210.

[4]   a) A. Servant, F. Qiu, M. Mazza, K. Kostarelos, B. J. Nelson, *Adv. Mater.* **2015**, *27*, 2981; b) B. E. de Avila, P. Angsantikul, J. Li, M. Angel Lopez-Ramirez, D. E. Ramirez-Herrera, S. Thamphiwatana, C. Chen, J. Delezuk, R. Samakapiruk, V. Ramez, M. Obonyo, L. Zhang, J. Wang, *Nat. Commun.* **2017**, *8*, 272; c) W. Gao, R. Dong, S. Thamphiwatana, J. Li, W. Gao, L. Zhang, J. Wang, *ACS Nano* **2015**, *9*, 117.

[5]   G. G. Genchi, L. Ceseracciu, A. Marino, M. Labardi, S. Marras, F. Pignatelli, L. Bruschini, V. Mattoli, G. Ciofani, *Adv. Healthcare Mater.* **2016**, *5*, 1808.

[6]   a) P. TirgarBahnamiri, S. Bagheri-Khoulenjani, *Med. hypotheses* **2017**, *102*, 56; b) E. E. Hunter, E. W. Brink, E. B. Steager, V. Kumar, *IEEE Robot. Autom. Lett.* **2018**, *3*, 1592; c) J.-y. Kim, S. Jeon, J. Lee, S. Lee, J. Lee, B. O. Jeon, J. E. Jang, H. Choi, *Sens. Actuator B Chem.* **2018**, *266*, 276; d) X. Wang, X. H. Qin, C. Hu, A. Terzopoulou, X. Z. Chen, T. Y. Huang, K. Maniura-Weber, S. Pané, B. J. Nelson, *Adv. Funct. Mater.* **2018**, *28*, 1804107; e) I. C. Yasa, A. F. Tabak, O. Yasa, H. Ceylan, M. Sitti, *Adv. Funct. Mater.* **2019**, 10.1002/adfm.201808992.

[7]   X.-Z. Chen, J.-H. Liu, M. Dong, L. Müller, G. Chatzipirpiridis, C. Hu, A. Terzopoulou, H. Torlakcik, X. Wang, F. Mushtaq, J. Puigmartí-Luis, Q.-D. Shen, B. J. Nelson, S. Pané, *Mater. Horiz.* **2019**, *6*, 1512.

[8]   a) X.-Z. Chen, M. Hoop, F. Mushtaq, E. Siringil, C. Hu, B. J. Nelson, S. Pané, *Appl. Mater.Today* **2017**, *9*, 37; b) X.-Z. Chen, B. Jang, D. Ahmed, C. Hu, C. De Marco, M. Hoop, F. Mushtaq, B. J. Nelson, S. Pane, *Adv. Mater.* **2018**, *30*, 1705061.

[9]   a) C. Ribeiro, V. Correia, P. Martins, F. M. Gama, S. Lanceros-Mendez, *Colloids Surf. B* **2016**, *140*, 430; b) F. Mushtaq, X.-Z. Chen, H. Torlakcik, C. Steuer, M. Hoop, E. Siringil, X. Marti, G. Limburg, P. Stipp, B. J. Nelson, S. Pané, *Adv. Mater.* **2019**, *31*, 1901378; c) K. Yue, R. Guduru, J. Hong, P. Liang, M. Nair, S. Khizroev, *PLoS One* **2012**, *7*, e44040; d) A. Rodzinski, R. Guduru, P. Liang, A. Hadjikhani, T. Stewart, E. Stimphil, C. Runowicz, R. Cote, N. Altman, R. Datar, S. Khizroev, *Sci Rep* **2016**, *6*, 20867; e) M. Nair, R. Guduru, P. Liang, J. Hong, V. Sagar, S. Khizroev, *Nat Commun* **2013**, *4*, 1707; f) C. L. Zhang, W. Q. Chen, S. H. Xie, J. S.

Yang, J. Y. Li, *Appl. Phys. Lett.* **2009**, *94*, 102907; g) J. Jin, S. G. Lu, C. Chanthad, Q. Zhang, M. A. Haque, Q. Wang, *Adv. Mater.* **2011**, *23*, 3853; h) J. Ma, J. M. Hu, Z. Li, C. W. Nan, *Adv. Mater.* **2011**, *23*, 1062; i) S. H. Xie, Y. M. Liu, Y. Ou, Q. N. Chen, X. L. Tan, J. Y. Li, *J. Appl. Phys.* **2012**, *112*, 074110; j) W. Eerenstein, N. D. Mathur, J. F. Scott, *Nature* **2006**, *442*, 759; k) R. Guduru, S. Khizroev, *Part. Part. Syst. Charact.* **2014**, *31*, 605.

[10]   X. Z. Chen, N. Shamsudhin, M. Hoop, R. Pieters, E. Siringil, M. S. Sakar, B. J. Nelson, S. Pané, *Mater. Horiz.* **2016**, *3*, 113.

[11]   J. Torgersen, X.-H. Qin, Z. Li, A. Ovsianikov, R. Liska, J. Stampfl, *Adv. Funct. Mater.* **2013**, *23*, 4542.

[12]   X.-H. Qin, A. Ovsianikov, J. Stampfl, R. Liska, *BioNanoMaterials* **2014**, *15*, 49.

[13]   a) J. J. Abbott, K. E. Peyer, M. C. Lagomarsino, L. Zhang, L. Dong, I. K. Kaliakatsos, B. J. Nelson, *Int. J. Robot. Res.* **2009**, *28*, 1434; b) A. Ghosh, P. Fischer, *Nano Lett.* **2009**, *9*, 2243.

[14]   J. Volatron, J. Kolosnjaj-Tabi, Y. Javed, Q. L. Vuong, Y. Gossuin, S. Neveu, N. Luciani, M. Hémadi, F. Carn, D. Alloyeau, F. Gazeau, *Sci. Rep.* **2017**, *7*, 40075.

[15]   P. B. Crino, J. Eberwine, *Neuron* **1996**, *17*, 1173.

[16]   a) D. Gorup, I. Bohacek, T. Milicevic, R. Pochet, D. Mitrecic, J. Kriz, S. Gajovic, *Neurosci. Lett.* **2015**, *597*, 176; b) T. M. Curtis, J. M. Hannett, R. M. Harman, N. A. Puoplo, G. R. Van de Walle, *Neurotoxicology* **2018**, *67*, 54.

[17]   a) A. Marino, S. Arai, Y. Y. Hou, E. Sinibaldi, M. Pellegrino, Y. T. Chang, B. Mazzolai, V. Mattoli, M. Suzuki, G. Ciofani, *ACS Nano* **2015**, *9*, 7678; b) M. Hoop, X.-Z. Chen, A. Ferrari, F. Mushtaq, G. Ghazaryan, T. Tervoort, D. Poulikakos, B. Nelson, S. Pané, *Sci. Rep.* **2017**, *7*, 4028; c) G. Ciofani, S. Danti, D. D'Alessandro, L. Ricotti, S. Moscato, G. Bertoni, A. Falqui, S. Berrettini, M. Petrini, V. Mattoli, A. Menciassi, *ACS Nano* **2010**, *4*, 6267.
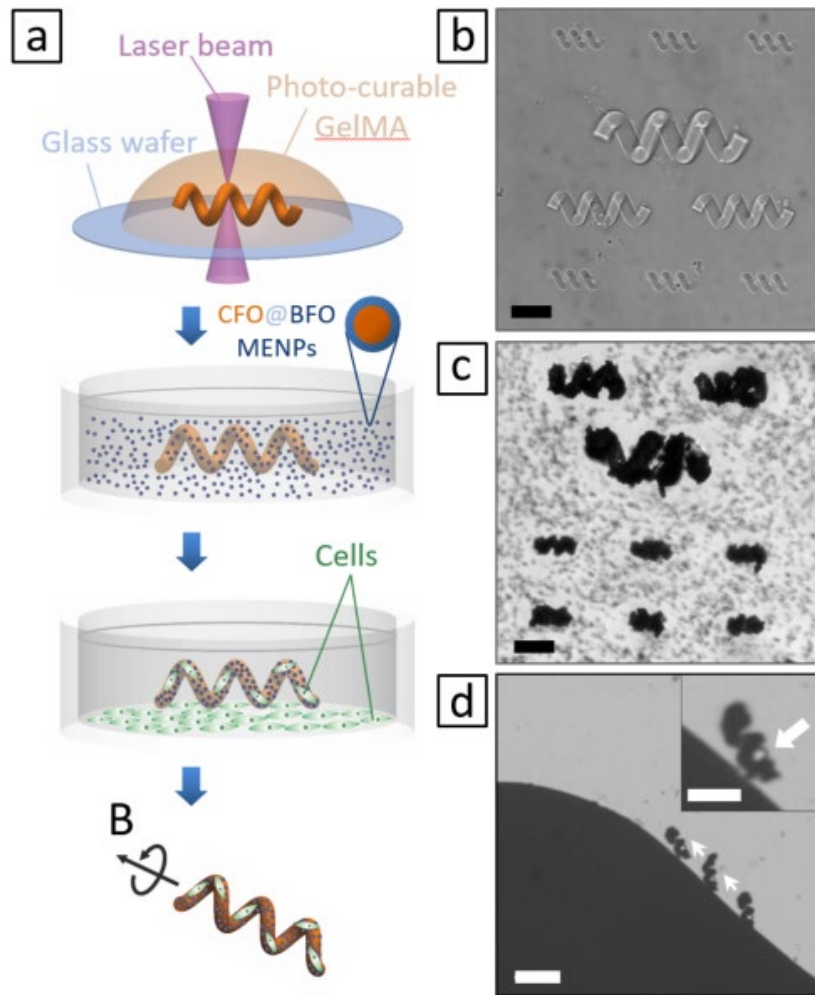
Figure 1. (a) Schematic illustration of the fabrication process of biodegradable soft helical microswimmers: two photon-polymerization (TPP) of GelMA helical microstructures; incubation of the helical microstructures in core-shell magnetoelectric nanoparticles (MENPs) dispersion; incubation of the cells on the ME soft helical microswimmers. Optical images of the helical microstructures fabricated using TPP (b) and the microswimmers decorated with MENPs (c). (d) The time-lapse image of a cell-laden helical microswimmer actuated under a rotating magnetic field in a microfluidic channel. The inset shows a magnified image of the helical swimmer with cells loaded as indicated by the white arrow. The scale bars in (b) (c) and the inset of (d) represents 50 μm; the scale bar in (d) represents 100 μm.
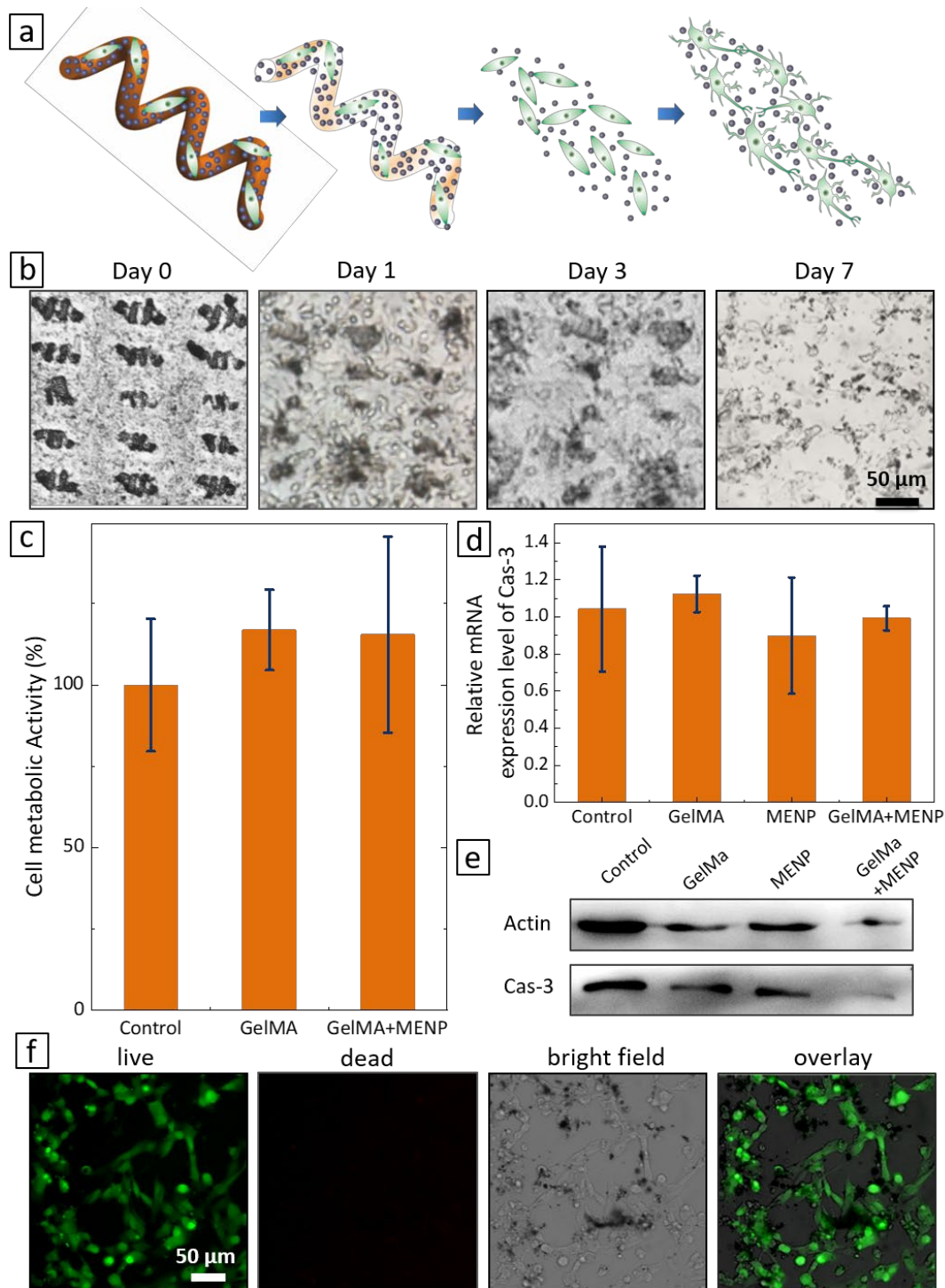
Figure 2. (a) Schematic illustration of the degradation process of the cell-laden soft microswimmers and induced neuronal differentiation of SH-SY5Y cells under magnetic stimulation. (b) Optical images showing the degradation process of the ME soft helical microswimmers after they were cultured with the cells for 0, 1, 3 and 7 days respectively. (c) Cell metabolic activity after 7 days of incubation with GelMA and GelMA+MENPs tested using the MTT assay. (d) The intracellular mRNA expression of Cas-3 after culture of SH-SY5Y with different group for 7 days (n = 3). (e) The intracellular level of Cas-3 in SH-SY5Y after culture with different group for 7 days. (f) Live-dead images after incubating SH-SY5Y cells with GelMA+MENPs microswimmers for 7 days. The live and dead cells are stained green and red, respectively.
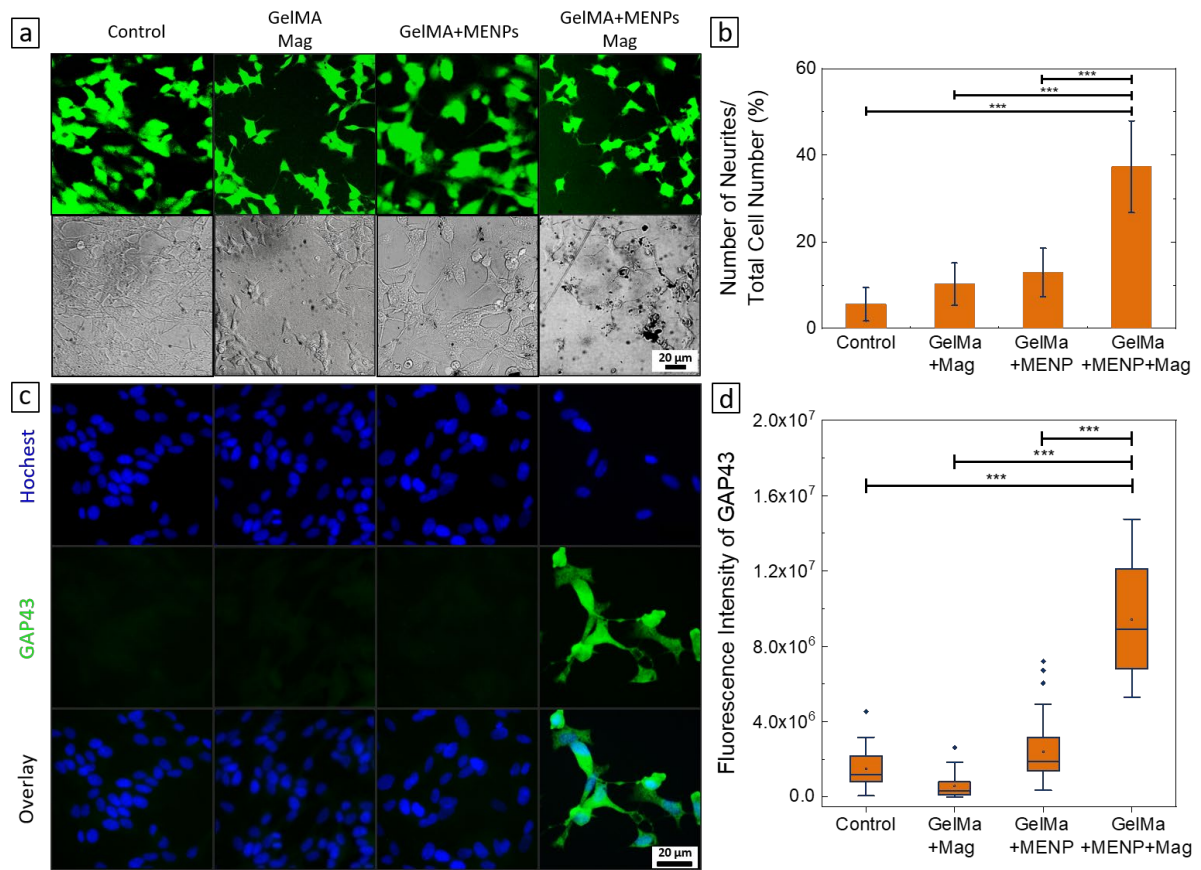
Figure 3. (a) Fluorescent and bright field microscopy images of the cells cultured at different conditions after 10 days. (b) Ratio of neurite numbers to the total cell number (***p < 0.001). (c) Fluorescent images of the cells cultured in different conditions. The nuclei are fluorescently stained in blue and the GAP 43 in green. (d) Box-and-whisker plots of the fluorescent intensities representing the level of GAP 43 expressed by in SH-SY5Y cells (***p < 0.001).

Biodegradable soft magnetoelectric microswimmers are fabricated with a 3D-printing technique. These microswimmers can perform targeted delivery of neuron-like cells and induce neuronal differentiation of these cells under different magnetic stimulation modes. This combinatorial technique presents a significant step towards highly integrated microrobots, and may open up new avenues for cell therapies.
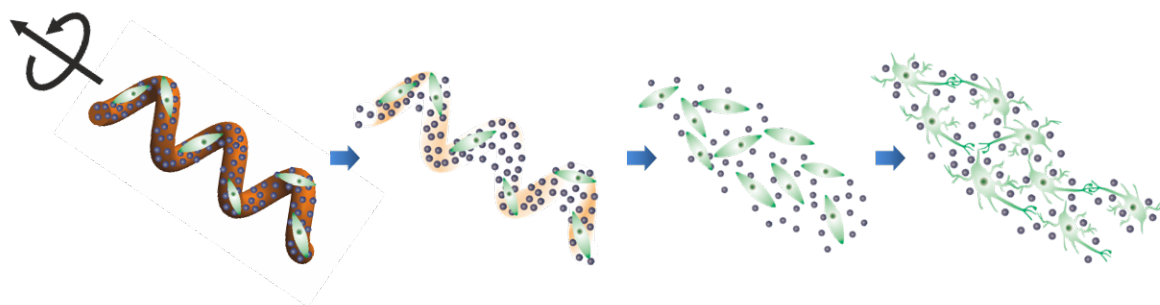
Keyword
soft robots, microrobots, piezoelectric, magnetoelectric, neuronal cell differentiation

M. Dong, X. Wang, X.-Z. Chen*, F. Mushtaq, S. Deng, C. H. Zhu, H. Torlakcik, A. Terzopoulou, X.-H. Qin, X. Xiao, J. Puigmartí-Luis, H. Choi, A. P. Pêgo, Q.-D. Shen, B. J. Nelson, and S. Pané*

3D-printed Soft Magnetoelectric Microswimmers for Delivery and Differentiation of Neuron-like cells

ToC figure

Supporting Information

3D-printed Soft Magnetoelectric Microswimmers for Delivery and Differentiation of Neuron-like cells

Mei Dong, Xiaopu Wang, Xiang-Zhong Chen*, Fajer Mushtaq, Siyu Deng, Caihong Zhu, Harun Torlakcik, Anastasia Terzopoulou, Xiao-Hua Qin, Xuanzhong Xiao, Josep Puigmartí-Luis, Hongsoo Choi, Ana Paula Pêgo, Qun-Dong Shen*, Bradley J. Nelson, and Salvador Pané*

1. Experimental Section

Synthesis of CFO@BFO Core-Shell Magnetoelectric Nanoparticles:

The synthesis of the CFO core was achieved using a hydrothermal synthesis adapted from [1]. $FeCl_3 \cdot 6H_2O$ and $CoCl_2$ were added to DI water together with cetyltrimethylammonium bromide (CTAB) to form a uniform solution with a concentration of 2.5 w/v %, 0.6 w/v % and 5 w/v%, respectively. Then 6M sodium hydroxide (NaOH) solution was rapidly added under vigorous stirring. A black dispersion was formed and the pH was raised to a value between 11-13. The dispersion was sonicated at room temperature for 30 minutes before being transferred to a Teflon autoclave and heated to 180 °C for 24 hours. The obtained particles were washed 3 times with DI water and 3 times with ethanol and then dried at 80 °C overnight. The BFO shells were coated on the CFO cores using the sol-gel method adapted from Javed et al. [2]. $(Fe(NO_3)_3 \cdot 9H_2O)$ and $Bi(NO_3)_3 \cdot 5H_2O$ was dissolved in Ethylene Glycol by stirring to form a solution with a final concentration of 0.405 w/v % and 0.537 w/v% respectively. The CFO nanoparticles were then added to the solution and mechanically stirred vigorously for 30 minutes at 60 °C. The mixture was then placed in an ultrasonic bath for 1 hour and left to dry overnight at 80 °C until all the liquid had evaporated. The resulting powder of CFO@BFO core-shell nanostructures was collected with a magnet and annealed for 2 hours at 600 °C.

Structure Characterization of CFO@BFO Core-Shell Magnetoelectric Nanoparticles:

Transmission electron microscopy (TEM, FEI F30) and scanning transmission electron microscopy (STEM, FEI Talos F200X) were employed to reveal the morphology of the NPs. Element distribution of the nanoparticles was revealed by HAADF STEM (FEI Talos F200X) equipped with energy-dispersive X-ray (EDX) mapping. X-ray diffraction (XRD) was performed on a Bruker AXS D8 Advance X-ray diffractometer (Cu target, wavelength of 1.542 Å).

M-E coupling of CFO@BFO Core-Shell Magnetoelectric Nanoparticles:

The local piezoresponse loops were measured using piezoresponse force microscopy (PFM, NT-MDT Ntegra Prima). A conductive AFM tip (FMG01/Pt) was used in contact mode to apply an alternating voltage (0.5 V) to the CFO@BFO NP and induce piezoelectric surface oscillations, which were sensed through the cantilever deflection. Local piezoresponse hysteresis loops were obtained at random locations of a NP by sweeping the applied DC bias, while simultaneously measuring the phase and amplitude response. The excitation voltage waveform was programmed to be a stepwise increasing pulsed DC voltage that was superimposed on a small AC voltage. In order to minimize the possible interference caused by electrostatic forces, the AC response signal was acquired only during the off-phase of the voltage pulse sequence. To study change in piezoelectric response of the sample under magnetic field, an in-plane magnetic field of 1000 Oe was applied to the sample.

Fabrication of GelMA+MENPs helical microswimmers:

The photoresist was prepared by dissolving GelMA (0.2 g/ml) and photoinitiator (P2CK 1.1 mg/ml) in PBS at 45 ºC. A 3D direct writing system (Nanoscribe, from Nanoscribe GmbH) was used to fabricate the GelMA helical frame of microswimmers. The GelMA helical structures were fabricated by controlling a near-infrared femtosecond laser (780 nm) scanning inside the photoresist following a preset trajectory. The sample was developed in water at 45 ºC for 0.5 hour to remove the unpolymerized photoresist. Afterwards, the sample was immersed in a 1% (1g/100ml) CFO@BFO water suspension with Tween (0.5 wt%) for 1 hour to load the nanoparticles.

Swimming of microswimmers under magnetic actuation:

A magnetic manipulation setup, which consists of three pairs of orthogonal Helmholtz coils, was used to control the GelMA+MENPs helical microswimmers movement. A sample

consisting of many microswimmers and a silicon wafer with micro-channel pattern was immersed in water in a sample holder. The sample holder was then placed at the center of the Helmholtz setup for the uniformity of the magnetic field. A microprobe (T-4-22, GGB Industries, INC.) was used to transport helical microswimmers to the micro-channel on the silicon wafer under water or artificial cerebrospinal fluid (ACSF). The ACSF was composed of 0.14 mol/ml NaCl, 0.005 mol/ml KCl, 0.002 mol/ml $CaCl_2$, 0.01 mol/ml HEPES, and 0.01 mol/ml D-glucose, and pH was adjusted to be 7.4 using KOH.[3] The helical microswimmers were manipulated to swim with varying speeds in different directions by controlling the direction and the rotating frequency of the magnetic field. The videos were recorded with a CCD camera at a frame rate of 30 fps. The position was abstracted by analyzing the video using Fiji to calculate the swimming speed together with the time information.

The swimming experiments of the cell-laden helical microswimmers in PBS or in the cell culture media were conducted using a magnetic actuation system (MFG-100-I, magnetbotiX AG, Switzerland), together with an integrated inverted optical microscope (Olympus IX-81), to control and record the videos under either bright field or the fluorescent microscope.

SH-SY5Y Cells cultured on GelMA+MENP microswimmers and swimming with microswimmers:

 The human neuroblastoma cells SH-SY5Y were preserved in 45% Dulbecco's minimum essential medium (DMEM) (Gibco, catalog no. 11965-092) and 45% Minimum Essential Medium (MEM)(Gibco, catalog no. 41090-036) supplemented with 10% fetal bovine serum (FBS; Gibco, catalog no. 10270-106), penicillin (100 U/ml), and streptomycin (100 U/ml; Invitrogen, catalog no. 15240-062) at 37 °C in a humidified atmosphere of 5% CO_2. Typically, the SH-SY5Y cells were subsequently trypsinized and re-suspended at a concentration of 6 × 10^6 cells/ml for cell seeding. The density of the cells on the microswimmers' body can be controlled to a certain extent by adjusting the seeding density of the cells. The microswimmers

were sterilized with 75% ethanol for 30 minutes and then washed three times with PBS. Subsequently, SH-SY5Y cells were seeded into a culture dish containing the microswimmers. The dish with cells and microswimmers was stored in an incubator overnight. After the SH-SY5Y cells were adhered to the microswimmers, the SH-SY5Y cells were dyed with a LIVE/DEAD™ Cell Imaging Kit (Invitrogen™, catalog no. R37601) for 30 minutes both before and after swimming with microswimmers.

Degradation of microswimmers with SH-SY5Y cells:

The SH-SY5Y cells were subsequently trypsinized and re-suspended at a concentration of 3×10^6 cells/ml for cell seeding. The microswimmers were sterilized with 75% (v/v) ethanol in water for 30 minutes and were washed three times with PBS. Subsequently, SH-SY5Y cells were seeded into a culture dish containing the microswimmers. The images of degradation were taken at the 0, 1st, 3rd, 7th day, and the SH-SY5Y cells were dyed with a LIVE/DEAD™ Cell Imaging Kit (Invitrogen™, catalog no. R37601) for 30 minutes on the 7th day.

The cell metabolic activity (reflecting cytotoxicity) test with MTT assay:

SH-SY5Y cells were seeded in 48-well plates at a density of 8×10^4 cells/well and incubated with GelMA and GelMA+MENPs for 7 days. The cytotoxicity was reflected by cell metabolic activity measured with an MTT assay. After incubation, 200 μL of MTT (0.5 mg/mL in pH 7.4 PBS) was added and incubated for another 4 hours; the medium was then replaced with 150 μL DMSO. The UV absorbance intensity of cells was measured by Microplate Reader (Infinite M200 Pro, Tecan AG) at 570 nm. Data is presented as a percentage in relation to the control group (SH-SY5Y cells seeded in 48-well plates at a density of 8×10^4 cells/well without GelMA or GelMA+MENPs for 7 days).

Microswimmers stimulating SH-SY5Y cells under magnetic fields and study of cell morphology:

The SH-SY5Y cells were trypsinized and re-suspended at a concentration of 1×10^5 cells/ml for seeding. The 48 well cell culture plate containing the SH-SY5Y cells and GelMA and GelMA+MENPs microswimmers was stored in an incubator overnight. After the SH-SY5Y cells adhered onto the microswimmers, the GelMA and GelMA+MENPs groups were placed under alternating magnetic fields (500 Oe, 1053.4Hz) for 30 minutes at 37 °C with a 5% CO_2 supply. The cells were stimulated by the magnetic field twice per day for 3, 7 and 10 days respectively. The other control groups were cultured with SH-SY5Y cells without magnetic field stimulation for 3, 7 and 10 days respectively. For negative control experiments, SH-SY5Y cells were cultured in a 48 well plate in normal media. SH-SY5Y cells were observed on the 3rd, 7th and 10th days and dyed with a LIVE/DEAD™ Cell Imaging Kit (Invitrogen™, catalog no. R37601). Cell differentiation was assessed as previously described. [4] Briefly, the ratio of the total number of neurites to the total cell number was calculated at 3, 7, 10 days of culture, respectively. The quantitative results of neurite outgrowth were obtained by analyzing microscopy images in Fiji (National Institute of Health, USA) software. For counting the number of neurites, at least 400 cells were analyzed. To be considered a neurite, a cell extension had to be twice longer than the average of cell diameters.

RT-PCR:

Total RNA was extracted from the cells by using Trizol reagent (Invitrogen) according to the supplier's protocol;[6] and 2.0 mg total RNA were reverse-transcribed into cDNA using PrimeScript RT reagent kit with gDNA eraser (Takara, Japan). Transcription levels of indicated genes and actin were measured by real-time RT-PCR by using SYBR PCR master mix (TakaRa, Japan) with indicated primers (Table S1).

Western Blot Analysis:

The proteins were separated by 15% SDS-PAGE. Rabbit anti-actin (1:5000, Abcam, ab8226) antibodies and anti- Caspase-3 (1:2000, Abcam, ab32351) were used as primary antibodies. Goat peroxidase-conjugated goat anti-rabbit IgG (1:5000, Abcam) was used as the secondary antibody.

Animals model and hematoxylin and eosin (HE) staining:

The animals were treated in accordance with the Guide for Care and Use of Laboratory Animals, approved by the Model Animal Research Center (MARC) of Nanjing University. Male c57 mice (6 weeks old) were purchased from MARC of Nanjing University. C57 mice received care underpathogen-free conditions. C57 mice were kept at 25 ± 1 °C and $50 \pm 5\%$ of humidity, and allowed free access to sterilized tap water and laboratory rodent chow. All the animal operations complied with the institutional and Chinese government guidelines for the care and use of experimental animals. Before surgery, the mice were weighed, anesthetized with isoflurane, and put into a stereotaxic apparatus. The cranium was exposed with a mid-sagittal incision. A hole was drilled with a dental drill mounted in the stereotaxic frame over the striatum area to the following coordinate: bregma +0.8 mm; lateral, +1.5mm. A micro-injector containing the nanoparticles (0.2%) was lowered 4.0 mm to cerebral ventricle, and 5 μL solution was injected over 5 min. For the HE staining, the formalin-fixed brains were prepared by Nanjing Drum Tower Hospital, and observed by fluorescence microscope (IX71, Olympus).

Immunofluorescence of SH-SY5Y cells:

Indirect immunofluorescence was operated as previously described.[5] The SH-SY5Y cells were cultured in different groups on a 20 mm confocal dish (glass bottom dish) and washed twice with PBS. They were then fixed in 4% paraformaldehyde for 30 minutes on ice and permeabilized with 0.15% Triton X-100. The SH-SY5Y cells were incubated with the GAP43

(Abcam, ab75810) primary antibody and the fluorescent secondary antibody (Abcam, ab96899). Nuclei were stained with Hoechst 33258 (Sigma B1155).

Immunofluorescence staining of brain tissue:

Brains were washed with PBS twice, then the tissue was placed in 4% paraformaldehyde for 6-8 hours, and subsequently transferred to 20% sucrose. 8–10 μm thick sections were obtained by freezing microtome (Thermo, CRYOSTAR NX50). The frozen section were washed with PBS three times, and blocked with 2% BSA at room temperature or 37 °C for 1 h, and incubated overnight at 4 °C with the primary antibody Caspase-3 (1:500, Abcam, ab32351), a MAP-2 (1:100, Abcam, ab183830) and the fluorescent secondary antibody (Abcam, ab150080 for Cas-3 and Abcam, ab96899 for MAP-2 respectively, concentration 1:1000) at room temperature. Nuclei were stained with Hoechst 33258 (Sigma B1155). Images were recorded by confocal laser scanning microscope (Zeiss LSM 710).

Statistical analysis.

All quantitative measurements are expressed as mean values, and error bars indicate the standard deviation of the mean unless otherwise stated. Statistical significance was performed using non-parametric Kruskal-Wallis test. Statistical significance was set at $p < 0.05$.

2. The structure and magnetoelectric coupling of ME Core-Shell Nanoparticles
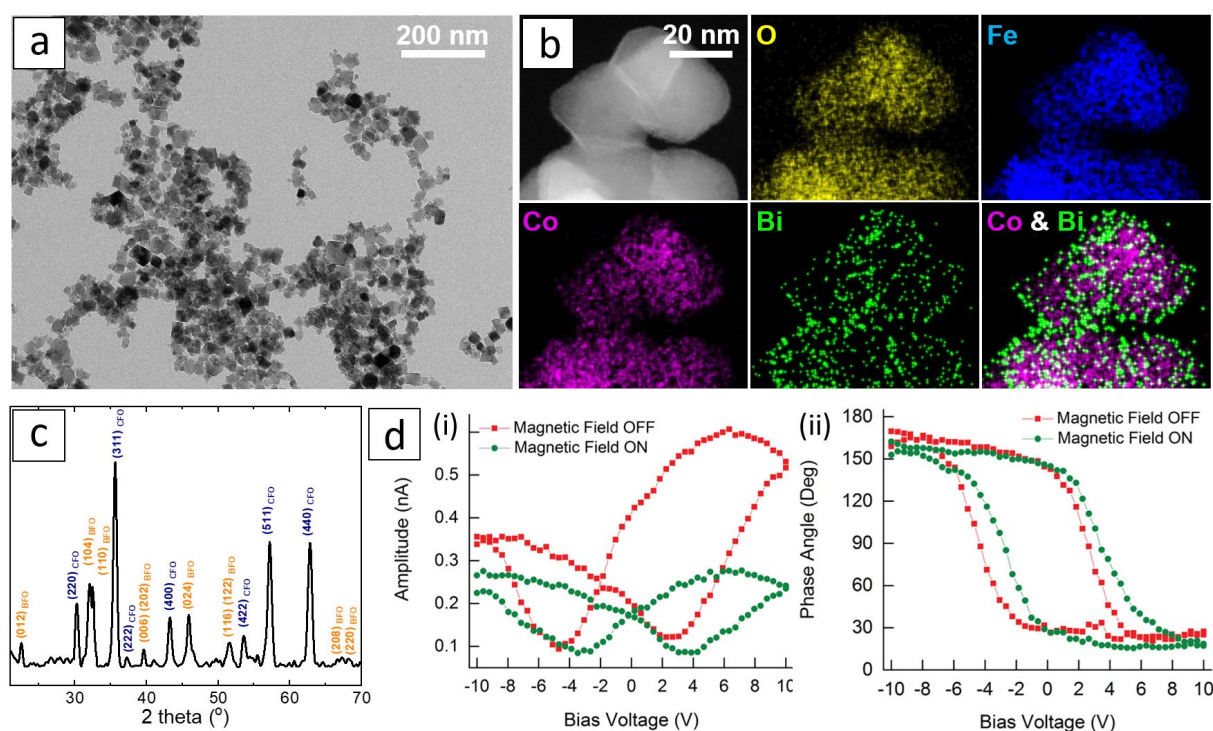
Figure S1. (a) TEM image of a large number of the core-shell magnetoelectric nanoparticles. (b) STEM images and EDX mappings of core-shell magnetoelectric nanoparticles. (c) An X-Ray Diffraction pattern of core-shell magnetoelectric nanoparticles powders. (d) Piezoresponse amplitude (i) and phase (ii) loops obtained from one type of CFO@BFO core-shell nanoparticles with (red) and without (green) magnetic field. (Panels (b), (c), and (d) are adapted from Ref [7], Copyright Wiley).

Figure S1a shows a large number of the core-shell magnetoelectric nanoparticles. The core-shell CFO@BFO NPs have an average size of 42 nm. The core-shell structure can be observed through the EDX mapping. As shown in Figure S1b, the cobalt, which only exists in CFO, is mostly surrounded by the bismuth. The crystalline structure of the CFO@BFO NPs was analyzed using X-ray diffraction (XRD). XRD patterns (Figure S1c) shows that the peaks are assigned to the Fd3m structure of $CoFe_2O_4$ (JCPDS No. 01-1121) and R3c structure of $BiFeO_3$ (JCPDS No. 71-2494).

The magnetoelectric coupling of core-shell nanoparticles was obtained by comparing the local piezoresponse loops with and without applying an external magnetic field of 1000 G. The polarization direction of the BFO can be switched by the DC bias applied through the tip. The

coercive voltages for the BFO shell measured without magnetic field were -4.7 V and 2.7 V, respectively. When we applied the magnetic field, the coercive voltages was changed to -3.5 V and 3.0 V, respectively. The magnetic field-induced changes in the coercive voltages indicate that the strain generated in the CFO (magnetostrictive phase) was transferred to the BFO (piezoelectric phase), facilitating the polarization reversal process in BFO. The change in positive coercive voltage is smaller than that of the negative voltage. The asymmetric change means that there is an offset of the center of the piezoresponse loop under the magnetic field, which is supposed to be caused by an electric field generated by the magnetoelectric effect. This is an evidence magnetoelectric effect mediated by strain in the core-shell CFO@BFO NPs.

3. Motion of the helical microswimmers

The microswimmers performed a corkscrew motion when actuated by low magnitude rotating magnetic fields. Due to the high friction between the microswimmers and the substrate surface, the microswimmers not only moved forwards, but also drifted towards the lateral direction while swimming, as shown in Figure S2 and Video SV1.
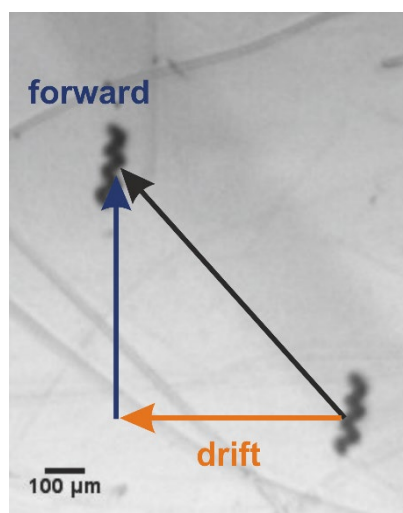
Figure S2. Time-lapsed screenshots of a video showing a helical microswimmer swimming in DI water under a rotating magnetic field with a magnitude of 2mT.

When the magnetic field was applied at a low rotating frequency, the microswimmer showed a wobbling motion. The drift velocity was very high and the forward velocity was very low. As the rotating frequency of the magnetic field increased, the forward velocity increased significantly and the influence of the drifting effect was reduced. Swimming then stabilized in the corkscrew motion with the increase in frequency. As the rotating frequency of the external magnetic field increased, the velocity of the microswimmers also increased until the step-out frequency was reached, subsequently the velocity decreased. Figure S3 shows the forward and drift velocity of a GelMA+MENPs microswimmer controlled by rotating magnetic fields with different magnitudes. We can see that the step out frequencies and the maximum velocities increased with the increasing magnitude of magnetic fields.
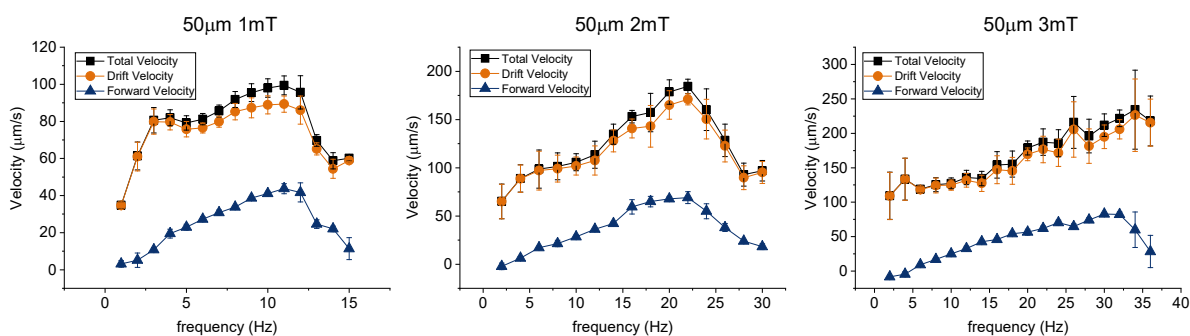
28

Figure S3. Frequency-dependent velocity analysis of GelMA+MENPs helical microswimmers with a length of 50 μm actuated at different rotating frequencies.

The structure size also influences the locomotion of the microswimmer, the step-out frequency of 100 μm long microswimmers is lower than that of 50 μm long microswimmers, as shown in Figure S4. However, the maximum velocity of 100 μm long swimmers is higher than that of the 50 μm swimmers.
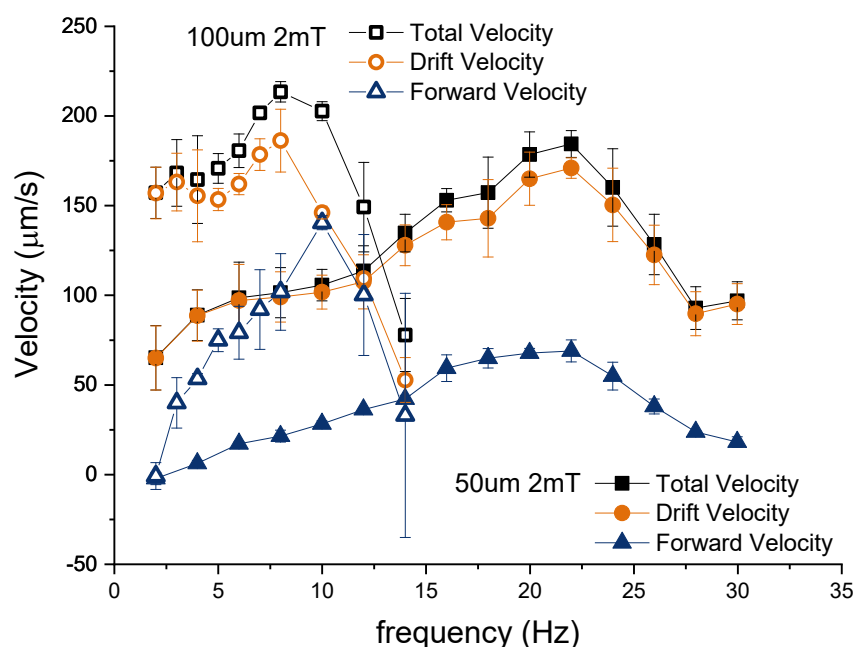

Figure S4. Frequency-dependent velocity analysis of GelMA+MENPs helical microswimmers of different size at 2 mT.
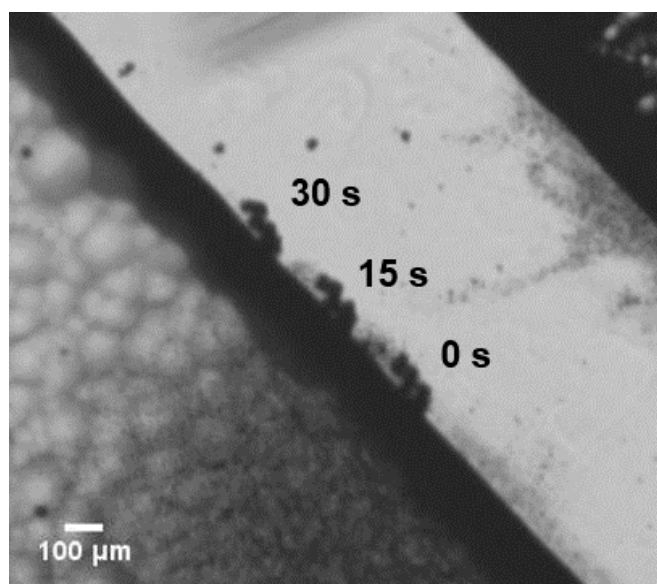
Figure S5. A time-lapse image of a GelMA+MENPs helical microswimmer actuated under a rotating magnetic field in a microfluidic channel.
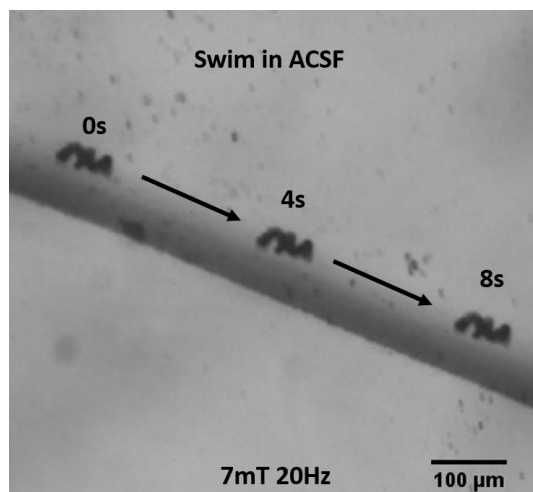
Figure S6. A time-lapse image of a GelMA+MENPs helical microswimmer actuated under a rotating magnetic field in artificial cerebrospinal fluid (ACSF).

4. Additional results of bio-related experiments of GelMA+MENPs helical microswimmers
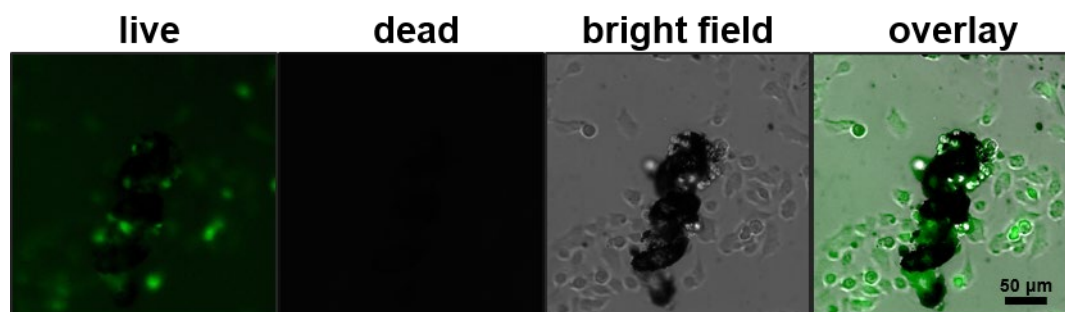

Figure S7. After a cell-laden helical swimmer swam for 30 minutes in a cell culture plate, the cells on the swimmer (SH-SY5Y) were processed for the live-dead assay. The live and dead cells are fluorescently stained green and red, respectively.
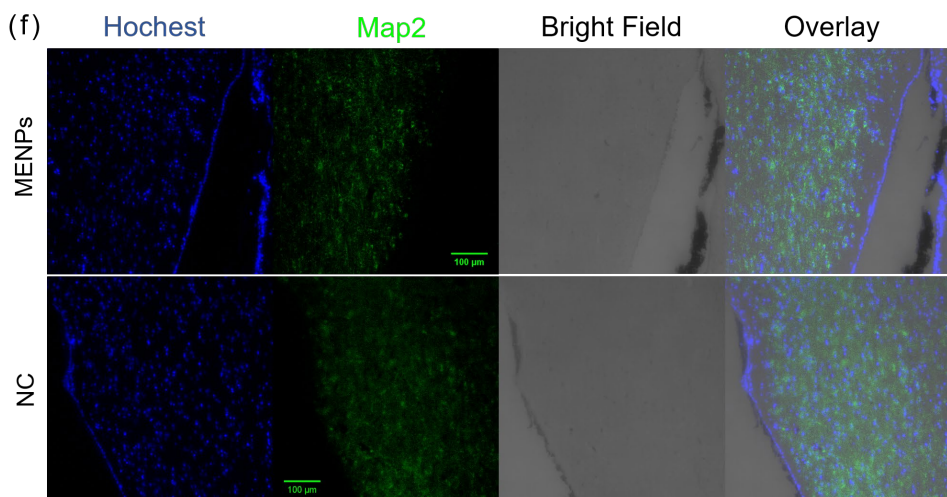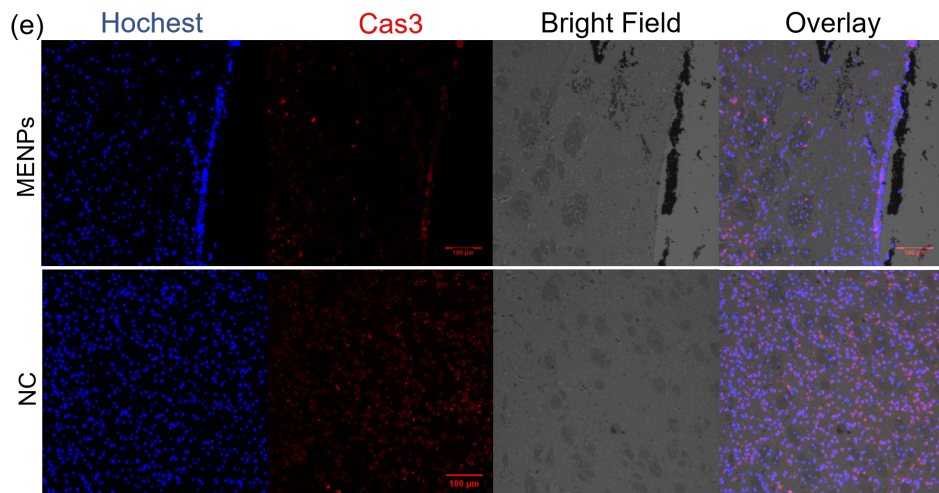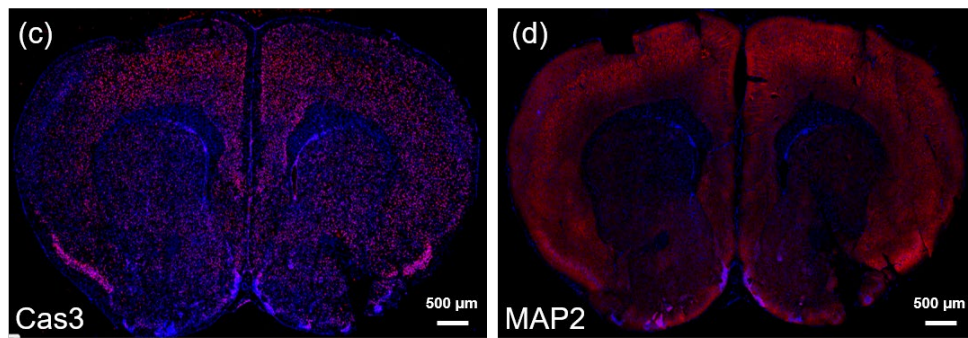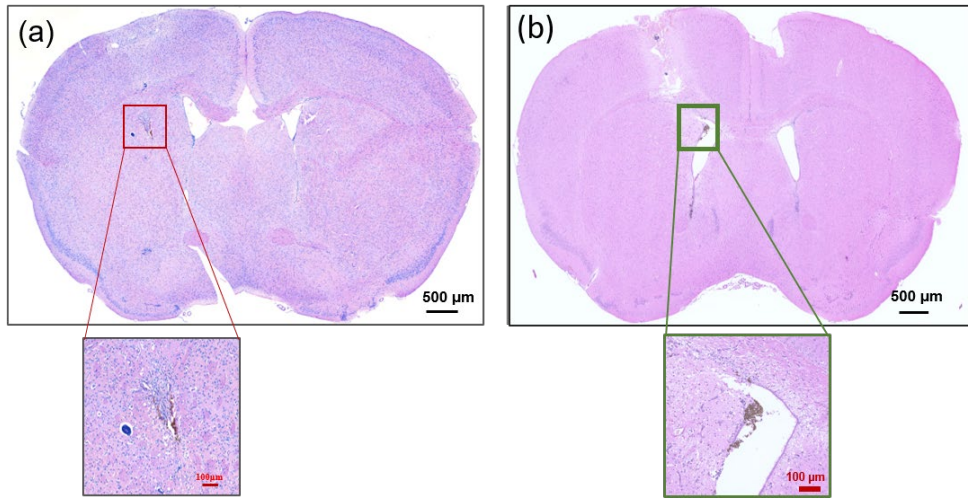
Figure S8. Histological observation of the brain tissues stained with H&E after injection of MENPs for 15 days (a), and for 3 days (b). The inset on the right shows the injection point. As observed, no signs of inflammation are visible around the injection site. (c) and (d) Immunofluorescence staining for Cas3 (c) and MAP2 (d) in a mouse brain after 15 days. (e) and (f) Immunofluorescence staining for Cas3 (c) and MAP2 (d) in a mouse brain after 3 days.

To further investigate the possibility of using MENPs in the body, we have preliminary tested the influence of MENPs on the brain of mice in vivo. In these experiments, 5 µL of MENP physiological saline water dispersion were injected to the striatum area of each mouse. Six male c57 mice (6 weeks old) were treated with 0.2 wt% MENPs. All of the mice survived 15 days. The hematoxylin and eosin (H&E) staining of the brain tissue sections were used to estimate the inflammation with diverse formulations. After 15 days, we found that the images of H&E-stained brain tissue show a non-distinctive character (Figure S8 (a)), which means that no cell apoptosis occurred around the injection site. Indeed, we also examined the expression of Cas3 in this region (Figure S8 (c)). The expression of Cas3 of the left hemisphere was not upregulated compared to that expressed in the right one, which means MENPs did not induce severe apoptosis of cells. Microtubule-associated protein 2 (MAP2) is known as the marker of specificity of mature neurons, and the loss of MAP2 was employed to judge the degree of neuronal injury. The expression of MAP2 also did not show significant difference between the two hemispheres (Figure S8 (d)). Therefore, all these results clearly show that MENPs have a good biocompatibility in vivo at this concentration. Similar results were also found after 3 days of injection (Figure S8 (b), (e), and (f)). These data indicate no acute inflammation and cell apoptosis.
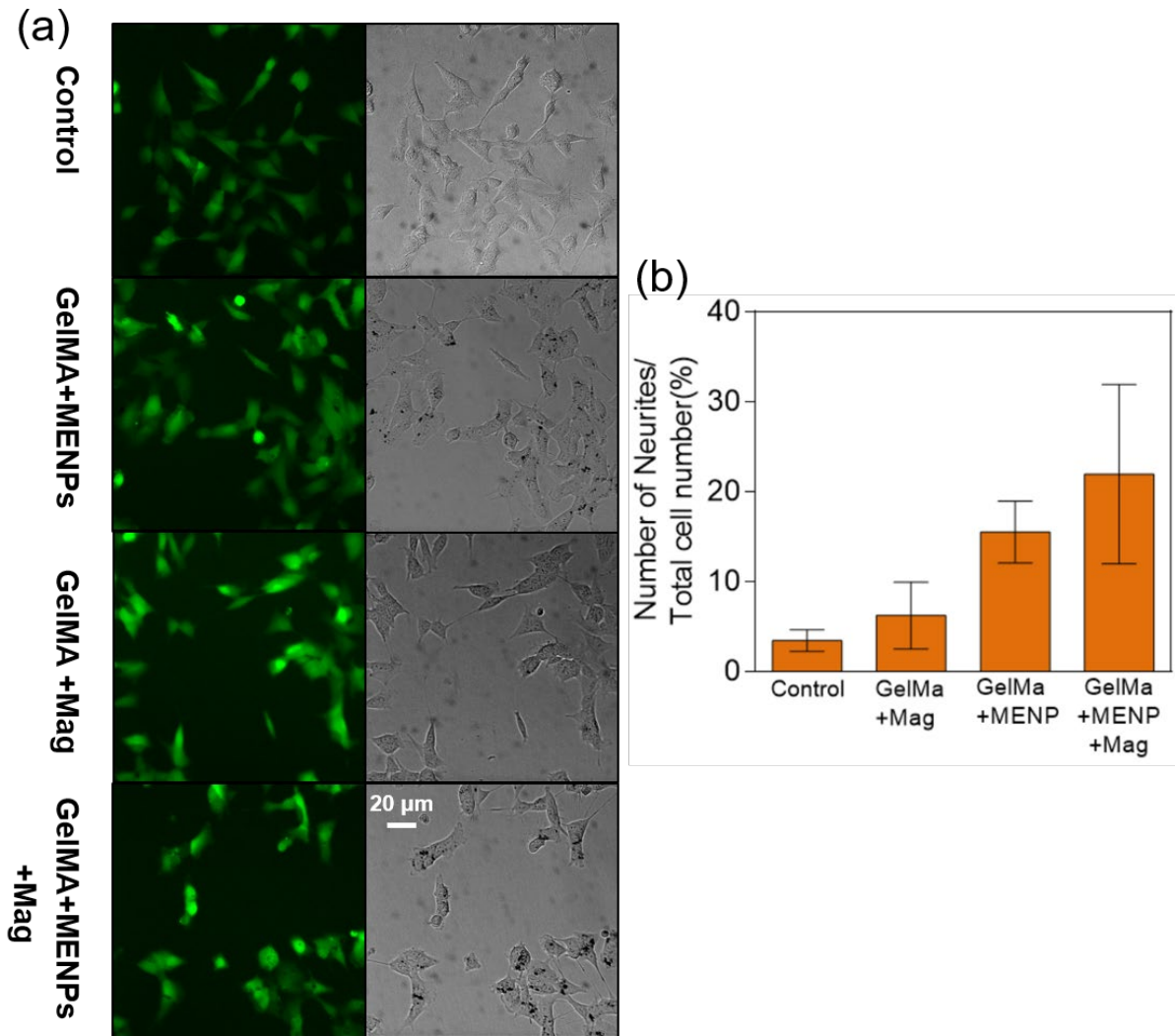
Figure S9. (a) Fluorescent and bright field microscopy images of SH-SY5Y cells cultured under different conditions for 3 days. (b) The ratio of the neurite number to the total cell number of cells cultured under different conditions.
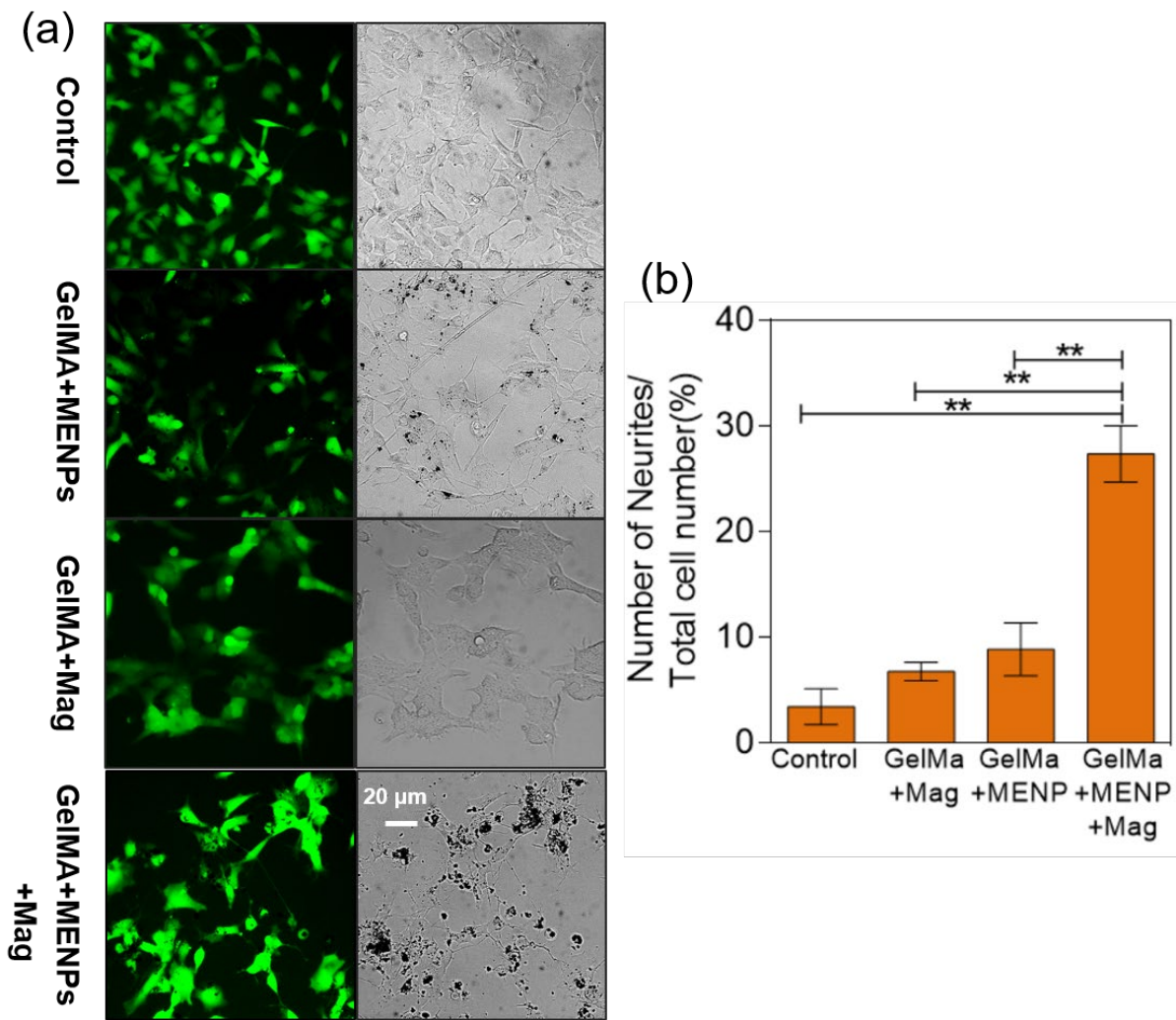
Figure S10. (a) Fluorescent and bright field microscopy images of SH-SY5Y cells cultured under different conditions for 7 days. (b) The ratio of the neurite number to the total cell number of cells cultured under different conditions (** for $p < 0.01$).
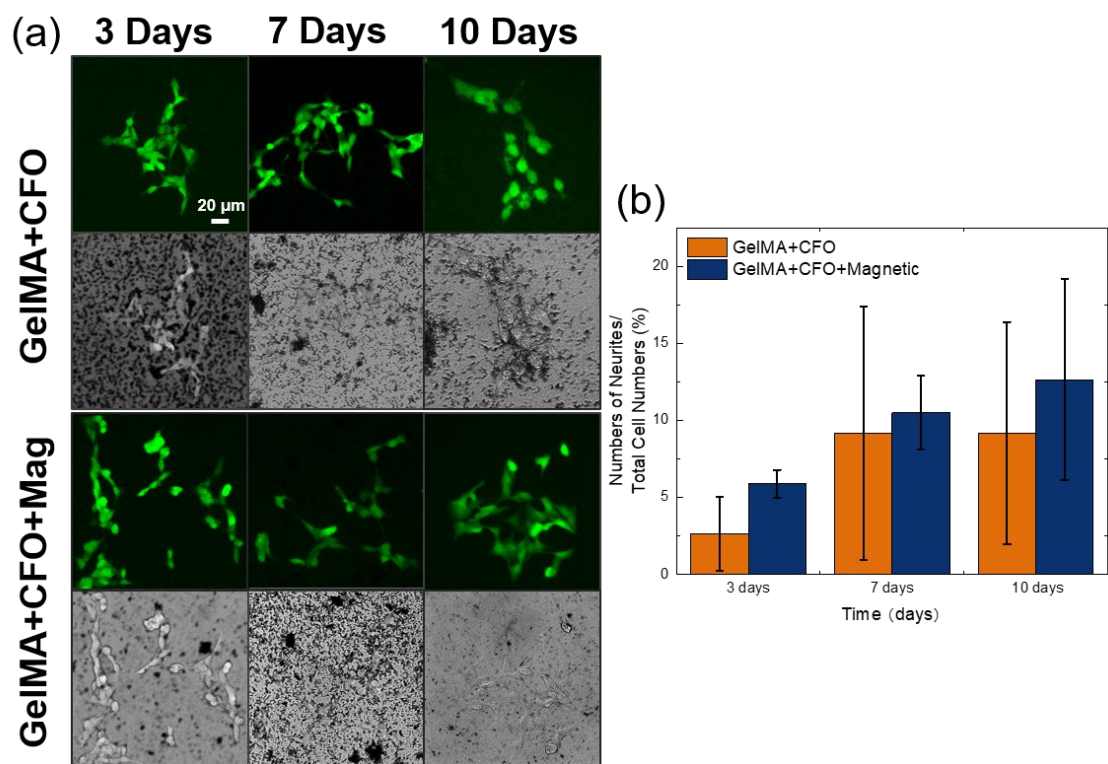
Figure S11. (a) Fluorescent and bright field microscopy images of the cells cultured with GelMa and CFO with or without magnetic field stimulating for 3, 7 and 10 days. (b) The ratio of the neurite number to the total cell number of cells cultured under different conditions.

Table S1. Primers used in this study

Strand/Gene	Primer	Sequence (5'-3')
Actin(Human)	Actin-F	CATGTACGTTGCTATCCAGGC
	Actin-R	CTCCTTAATGTCACGCACGAT
Caspase3(Human)	Caspase3-F	GAACTGGACTGTGGCATTGAGA
	Caspase3-F	CACAAAGCGACTGGATGAACC

References for supporting information:

[1] G. B. Ji, S. L. Tang, S. K. Ren, F. M. Zhang, B. X. Gu, Y. W. Du, *J. Cryst. Growth*, **2004**, *270*, 156.

[2] K. Javed, W. J. Li, S. S. Ali, D. W. Shi, U. Khan, S. Riaz, X. F. Han, *Sci. Rep.*, **2015**, *5*, 18203.

[3] A. Marino, S. Arai, Y. Y. Hou, E. Sinibaldi, M. Pellegrino, Y. T. Chang, B. Mazzolai, V. Mattoli, M. Suzuki, G. Ciofani, *ACS Nano* **2015**, *9*, 7678.

[4] D. Sandquist, T. H. Williams, S. K. Sahu, S. Kataoka. Morphological differentiation of a murine neuroblastoma clone in monolayer culture induced by dexamethasone. *Experimental Cell Research,* **1978,** 113, 375

[5] C. P. Wan, R.V. Sigh, B.H. Lau. *J. Immunol. Methods*. **1994**, *173*, 265

[6] M. Dong, X. Z. Xiao, Z. G. Su, Z. H. Yu, C. G. Qian, J. H. Liu, J. C. Zhao, Q. D. Shen, *Small* **2019**, *15*, e1900212.

[7] Mushtaq, F.; Chen, X.-Z.; Torlakcik, H.; Steuer, C.; Hoop, M.; Siringil, E.; Marti, X.; Limburg, G.; Stipp, P.; Nelson, B. J.; Pané, S., *Adv. Mater.* **2019**, 31, 1901378.